

A targeted coherent search for gravitational waves from compact binary coalescences

I. W. Harry^{1,*} and S. Fairhurst^{1,†}

¹*School of Physics and Astronomy, Cardiff University,
Queens Buildings, The Parade, Cardiff, CF24 3AA, UK*

We present the details of a method for conducting a targeted, coherent search for compact binary coalescences. The search is tailored to be used as a followup to electromagnetic transients such as Gamma Ray Bursts. We derive the coherent search statistic for Gaussian detector noise and discuss the benefits of a coherent, multi-detector search over coincidence methods. To mitigate the effects of non-stationary data, we introduce a number of signal consistency tests, including the null SNR, amplitude consistency and several χ^2 tests. We demonstrate the search performance on Gaussian noise and on data from LIGO’s fourth science run and verify that the signal consistency tests are capable of removing the majority of noise transients and the search gives an efficiency comparable to that achieved in Gaussian noise.

I. INTRODUCTION

There has been excellent progress towards gravitational wave astronomy over recent years. The first generation of large scale gravitational wave interferometers reached unprecedented sensitivities and have undertaken extended science runs. The U.S. Laser Interferometer Gravitational-wave Observatory (LIGO) [1], the French–Italian Virgo [2] and the German–British GEO600 [3] detectors now form a collaborative network of interferometers. The data from these detectors has been analyzed for gravitational waves from compact binary coalescence [4], stochastic background [5], unmodelled burst [6] and pulsar [7] sources. LIGO’s sixth science run (S6) and Virgo’s second and third science runs (VSR2 and VSR3) ended in October 2010 and yielded the most sensitive data yet taken; the analysis of this data is ongoing. In the meantime, the detectors are being upgraded to their advanced configurations [8–10], with the expectation of a ten fold improvement in sensitivity. With these sensitivities, it is expected that gravitational waves will be observed regularly [11]. Furthermore, with a proposed advanced detector in Japan [12], a possible detector in Australia [13], and 3rd generation detectors on the horizon [14], future prospects are promising.

As the gravitational wave community matures it is essential that a relationship is built between gravitational wave (GW) and electromagnetic (EM) astronomers. The GW emission from a source is likely to provide complementary information to emission in various EM bands, and a joint observation is significantly more likely to answer outstanding astrophysical questions. Already this relationship is beginning to mature. A number of EM transients have already been followed up in GW data [15–17]. Additionally, infrastructure is also being put in place to allow for EM follow-up of GW observations [18].

Compact binary coalescences (CBC) are one of the most promising sources of gravitational waves, and also

an ideal candidate for joint GW-EM astronomy. During the late stages of inspiral and merger, a compact binary emits a distinctive, “chirping” gravitational wave signal. Furthermore, CBCs containing at least one neutron star (NS) are expected to emit electromagnetically. Specifically, binary neutron stars (BNS) and neutron star–black hole binaries (NSBH) mergers are the preferred progenitor model for the short gamma-ray burst (GRB) [19, 20]. It is also possible that these mergers will be observable electromagnetically as orphan afterglows [19], optical [21] or radio transients [22]. Since GRBs are well localized both in time and on the sky by EM observations, the corresponding GW search can be simplified by reducing the volume of parameter space relative to an all-sky, all-time search. Targeted searches for CBC waveforms associated to short GRBs were performed using data from LIGO’s fifth science run (S5) and Virgo’s first science run (VSR1) [15, 16].

In this paper, we introduce a targeted, coherent search algorithm for detecting GW from CBC. This targeted search is designed as a follow-up to EM transients, and in particular GRBs. Previous searches for this source have made use of a coincidence requirement — namely that a signal with consistent parameters is observed in two or more detectors in the network. The analysis introduced here makes use of the data from all operational detectors, and combines the data in a coherent manner before matched filtering against CBC template waveforms. In a coherent analysis, it is straightforward to restrict the signal model to only two independent polarizations. This allows for the rejection of incoherent background noise, and consequently increases the sensitivity of the search if more than two detectors are operating.

The data output by gravitational wave interferometers is neither stationary nor Gaussian, but is contaminated by noise transients of instrumental and environmental origin. This makes the task of doing data analysis a complex one, and matched filtering alone is not sufficient to distinguish signal from noise. Regardless of whether a coincident or coherent search is performed, the most significant events by signal-to-noise ratio (SNR) would always be dominated by non-Gaussian transients, or “glitches”, in the data. A significant effort goes into understand-

* ian.harry@astro.cf.ac.uk

† stephen.fairhurst@astro.cf.ac.uk

ing the cause of these glitches [23] and removing times of poor data quality from the analysis. While these efforts greatly reduce the number of glitches they cannot remove them entirely. Therefore the analysis must also employ methods to distinguish signal from noise transients. In previous CBC searches, signal consistency tests [24, 25] have proved very effective at removing the non-Gaussian background. We extend these tests to the coherent analysis described in this paper and demonstrate their continued effectiveness. In addition, coherent analyses naturally lend themselves to multi-detector consistency tests, such as the null stream [26]. We describe a number of such consistency tests for this templated CBC search and again demonstrate their efficacy. Finally, we are able to show that the various signal consistency tests are sufficient to remove the majority of non-Gaussian transients and render the search almost as sensitive as if the data were Gaussian and stationary.

The layout of this paper is as follows. In section II, we describe the formulation of a targeted coherent triggered search for CBC signals. In section III we discuss an implementation of the null stream formalism and other multi-detector consistency tests. In section IV we describe a number of χ^2 tests than can be applied in a coherent search to try to separate and veto glitches. Finally, in V we outline an implementation of a targetted, coherent search for CBC and present results on both simulated, Gaussian data and real detector data taken from LIGO's fourth science run (S4).

II. COHERENT MATCHED FILTERING

In this section, we describe the coherent matched-filtering search for a gravitational wave signal from a coalescing binary in data from a network of detectors. We restrict attention to binaries where the component spin can be neglected. The description is primarily tailored towards searches where the sky location of the gravitational wave event is known a priori, as is appropriate when performing a followup of an EM transient such as a GRB [16, 19]. Finally, since all previously published CBC search results [4, 27, 28] have used a coincidence search between detectors, we compare the coherent analysis with the multi-detector coincident analysis.

The coherent analysis for coalescing binary systems has been derived previously using a similar method in [29–32]. Our presentation makes use of the \mathcal{F} -statistic formalism, introduced in [33]. This was originally defined as a method for performing searches for continuous wave searches and has been regularly used for this task (see for example [34]). It was noted in [35] that the \mathcal{F} -statistic and the multiple detector inspiral statistic derived in [30] are similar and the \mathcal{F} -statistic was adapted to searches for CBC signals in [36].

A. The binary coalescence waveform

The generic binary coalescence waveform depends upon as many as seventeen parameters. However, we restrict attention to binaries on circular orbits with non-spinning components. This reduces the parameter space to nine dimensions: the two component masses M_1 and M_2 ; the sky location of the signal (θ, ϕ) ; the distance, D , to the signal; the coalescence time of the signal, t_o ; the orientation of the binary, given by the inclination ι , the polarization angle ψ and the coalescence phase ϕ_o . We also assume that the sky location (θ, ϕ) of the signal is known, thereby reducing the number of unkown parameters to seven.

In the radiation frame, where the gravitational wave propagates in the \mathbf{e}_z^R -direction, the gravitational waveform is given by

$$\mathbf{h} = h_+ \mathbf{e}_+ + h_\times \mathbf{e}_\times \quad (2.1)$$

where

$$\begin{aligned} \mathbf{e}_+ &= \mathbf{e}_x^R \otimes \mathbf{e}_x^R - \mathbf{e}_y^R \otimes \mathbf{e}_y^R, \\ \mathbf{e}_\times &= \mathbf{e}_x^R \otimes \mathbf{e}_y^R + \mathbf{e}_y^R \otimes \mathbf{e}_x^R, \end{aligned} \quad (2.2)$$

and the waveforms $h_{+, \times}$ depend upon seven parameters $(M_1, M_2, t_o, D, \iota, \psi, \phi_o)$. The three remaining angles (ι, ψ, ϕ_o) give the relationship between the radiation frame and the source frame (in which \mathbf{e}_z^S lies in the direction of the binary's angular momentum and \mathbf{e}_x^S along the separation between the binary components at t_o). Even for a known sky location, it is necessary to search a seven dimensional parameter space of signals. Naively covering this space with a grid of templates would be prohibitively costly [37]. However, the analysis is greatly simplified by the observation that the last four parameters enter only as amplitude parameters which can be analytically maximized over at minimal cost.¹ Specifically, the two polarizations of the waveform can be expressed as

$$\begin{aligned} h_+(t) &= \mathcal{A}^1 h_0(t) + \mathcal{A}^3 h_{\frac{\pi}{2}}(t) \\ h_\times(t) &= \mathcal{A}^2 h_0(t) + \mathcal{A}^4 h_{\frac{\pi}{2}}(t). \end{aligned} \quad (2.3)$$

The two phases of the waveform are written as h_0 and $h_{\frac{\pi}{2}}$. These depend upon the physical parameters of the system (in this case just the masses) as well as the coalescence time t_o .² \mathcal{A}^i are constant amplitude terms and are given

¹ This was observed for the inspiral signal in [30] and independently for continuous wave signals in [33].

² This decomposition is actually valid for all binaries in which the plane of the orbit does not precess. Thus, binary coalescence waveforms in which the spins are aligned with the orbital angular momentum can also be expressed in this form. However, for generic spin configurations, the orbit will precess and this simple decomposition is no longer applicable.

explicitly as [32, 36]

$$\begin{aligned}\mathcal{A}^1 &= A_+ \cos 2\phi_o \cos 2\psi - A_\times \sin 2\phi_o \sin 2\psi \\ \mathcal{A}^2 &= A_+ \cos 2\phi_o \sin 2\psi + A_\times \sin 2\phi_o \cos 2\psi \\ \mathcal{A}^3 &= -A_+ \sin 2\phi_o \cos 2\psi - A_\times \cos 2\phi_o \sin 2\psi \\ \mathcal{A}^4 &= -A_+ \sin 2\phi_o \sin 2\psi + A_\times \cos 2\phi_o \cos 2\psi,\end{aligned}\quad (2.4)$$

where

$$\begin{aligned}A_+ &= \frac{D_o}{D} \frac{(1 + \cos^2 \iota)}{2} \\ A_\times &= \frac{D_o}{D} \cos \iota,\end{aligned}\quad (2.5)$$

and D_o is a fiducial distance which is used to scale the amplitudes \mathcal{A}^i and waveforms $h_{0,\frac{\pi}{2}}$. Thus, the amplitudes \mathcal{A}^i depend upon the distance to the source and the binary orientation as encoded in the three angles (ι, ψ, ϕ_0) . For *any* set of values \mathcal{A}^i , the expressions (2.4) can be inverted to obtain the physical parameters, unique up to reflection symmetry of the system [36].

The gravitational waveform observed in a detector X is

$$h^X = h^{ij} D_{ij}^X \quad (2.6)$$

where D_{ij}^X denotes the detector response tensor. For an interferometric detector, the response tensor is given by

$$\mathbf{D}^X = (\mathbf{e}_x^X \otimes \mathbf{e}_x^X - \mathbf{e}_y^X \otimes \mathbf{e}_y^X) \quad (2.7)$$

where the basis vectors \mathbf{e}_x^X and \mathbf{e}_y^X point in the directions of the arms of the detector. It is often convenient to re-express the gravitational wave signal observed in a given detector as

$$h^X(t) = F_+(\theta^X, \phi^X, \chi^X) h_+(t) + F_\times(\theta^X, \phi^X, \chi^X) h_\times(t), \quad (2.8)$$

where the detector response to the two polarizations of the gravitational wave is encoded in the functions

$$\begin{aligned}F_+(\theta, \phi, \chi) &= -\frac{1}{2}(1 + \cos^2 \theta) \cos 2\phi \cos 2\chi \\ &\quad - \cos \theta \sin 2\phi \sin 2\chi,\end{aligned}\quad (2.9)$$

$$\begin{aligned}F_\times(\theta, \phi, \chi) &= \frac{1}{2}(1 + \cos^2 \theta) \cos 2\phi \sin 2\chi \\ &\quad - \cos \theta \sin 2\phi \cos 2\chi.\end{aligned}\quad (2.10)$$

These response functions depend upon the three angles $(\theta^X, \phi^X, \chi^X)$ which relate the detector frame to the radiation frame: θ^X and ϕ^X give the sky location relative to the detector, while χ^X is the polarization angle between the detector and the radiation frames. We have, somewhat unconventionally, allowed for a polarization angle in transforming from source to radiation *and* radiation to detector coordinates. In what follows, we will often find it convenient to fix the angle χ^X by explicitly tying it to the detector (or geocentric) frame; for example, by maximizing the detector (or network) sensitivity to the

$+$ polarization. The angle ψ then describes the orientation of the source with respect to this preferred radiation frame.

Since we are considering CBC observed in ground-based detectors, the time that a potential signal would spend in the sensitivity band of any detector will be short (less than 60s for the initial detectors). Thus the change in the source's sky location over the observation time may be neglected, and the angles $(\theta^X, \phi^X, \chi^X)$ can be treated as constants. When working with a network of detectors, it is often useful to work in the geocentric frame. The location of the source (θ, ϕ, χ) is measured relative to this frame, and coalescence time is measured at the Earth's centre. In this case, the location and orientation of the detector X are specified by three angles, which we denote $\vec{\alpha}^X$, and the detector response will depend upon six angles $(\vec{\alpha}^X, \theta, \phi, \chi)$. Then, the observed signal in a given detector is³

$$h^X(t) = F_+(\vec{\alpha}^X, \theta, \phi, \chi) h_+(t^X) + F_\times(\vec{\alpha}^X, \theta, \phi, \chi) h_\times(t^X), \quad (2.11)$$

where t^X is the time of arrival of the signal at detector X ,

$$t^X = t - dt(\vec{\alpha}^X, \theta, \phi, \chi) \quad (2.12)$$

and dt gives the difference in arrival time of the signal between the geocenter and detector, for the given sky position.

Combining the final expressions for the binary coalescence waveform (2.3) and the detector response (2.11), we can express the gravitational waveform observed in a given detector as

$$h^X(t) = \sum_{\mu=1}^4 \mathcal{A}^\mu(D, \psi, \phi_o, \iota) h_\mu^X(t) \quad (2.13)$$

where the \mathcal{A}^μ are defined in (2.4) and h_μ^X are given by

$$\begin{aligned}h_1^X(t) &= F_+^X h_0(t^X) \\ h_2^X(t) &= F_\times^X h_0(t^X) \\ h_3^X(t) &= F_+^X h_{\frac{\pi}{2}}(t^X) \\ h_4^X(t) &= F_\times^X h_{\frac{\pi}{2}}(t^X).\end{aligned}\quad (2.14)$$

B. Multi detector binary coalescence search

Matched filtering theory [39] provides a method for determining whether the signal $h(t, \xi)$, parametrized by

³ We do not give the explicit formula for the response function dependent on the six angles $(\vec{\alpha}^X, \theta, \phi, \chi)$, as the expression is somewhat lengthy. It can be obtained by performing six successive rotations to the detector response tensor to transform from the detector frame, via the geocentric frame, to the radiation frame. The calculation is detailed in [38].

the time and other parameters ξ , is present in a noisy data stream. The data output by a detector is

$$s^X(t) = n^X(t) + h^X(t, \xi) \quad (2.15)$$

where $n^X(t)$ is the noise, taken to be Gaussian and stationary. The noise $n^X(t)$ of the detectors is characterized by the noise power spectral density (PSD) $S_h^X(f)$ as

$$\langle \tilde{n}^X(f)[\tilde{n}^X(f')]^\star \rangle = \delta(f - f')S_h^X(f). \quad (2.16)$$

With this, we define the single detector inner product between two time series $a(t)$ and $b(t)$ as

$$(a^X|b^X) = 4 \operatorname{Re} \int_0^\infty \frac{\tilde{a}^X(f)[\tilde{b}^X(f)]^\star}{S_h^X(f)}. \quad (2.17)$$

Then, the likelihood ratio of there being a signal h present in the data is given by:

$$\Lambda(h) = \frac{P(s|h)}{P(s|0)} = \frac{e^{-(s^X-h^X|s^X-h^X)/2}}{e^{-(s^X|s^X)/2}}, \quad (2.18)$$

and the log-likelihood can be written as

$$\log \Lambda = (s|h) - \frac{1}{2}(h|h). \quad (2.19)$$

The likelihood ratio for multiple detectors is a straightforward generalization of the single detector expression (2.18). Assuming that the noise in different detectors are independent, in the sense that

$$\langle \tilde{n}^X(f)[\tilde{n}^Y(f')]^\star \rangle = \delta^{XY}\delta(f - f')S_h^X(f), \quad (2.20)$$

the multi-detector inner product is simply given by the sum of the single detector contributions

$$(\mathbf{a}|\mathbf{b}) := \sum_X (a^X|b^X). \quad (2.21)$$

The multi-detector likelihood is given by

$$\ln \Lambda = (\mathbf{s}|\mathbf{h}) - \frac{1}{2}(\mathbf{h}|\mathbf{h}). \quad (2.22)$$

This is the optimal statistic for signal detection in Gaussian noise: the larger the value of $\ln \Lambda$, the more likely that a signal is present. It is not, however, an optimal statistic if the noise is not Gaussian, as we will explore in more detail in sections III and IV.

Specializing to the case of binary coalescence, we can substitute the known waveform parametrization (2.13) into the general matched filter likelihood (2.22). The multi-detector likelihood becomes

$$\ln \Lambda = \mathcal{A}^\mu(\mathbf{s}|\mathbf{h}_\mu) - \frac{1}{2}\mathcal{A}^\mu \mathcal{M}_{\mu\nu} \mathcal{A}^\nu \quad (2.23)$$

where the matrix $\mathcal{M}_{\mu\nu}$ is defined as

$$\mathcal{M}_{\mu\nu} := (\mathbf{h}_\mu|\mathbf{h}_\nu). \quad (2.24)$$

The derivative of (2.23) with respect to \mathcal{A}^μ provides the values of \mathcal{A}^μ which maximize the likelihood as

$$\hat{\mathcal{A}}^\mu = \mathcal{M}^{\mu\nu}(\mathbf{s}|\mathbf{h}_\nu), \quad (2.25)$$

where, following [40], we take $\mathcal{M}^{\mu\nu}$ to be the inverse of $\mathcal{M}_{\mu\nu}$. We then define the coherent SNR via the maximum likelihood as

$$\rho_{\text{coh}}^2 = 2 \ln \Lambda|_{\max} = (\mathbf{s}|\mathbf{h}_\mu)\mathcal{M}^{\mu\nu}(\mathbf{s}|\mathbf{h}_\nu). \quad (2.26)$$

It is not difficult to show that ρ_{coh}^2 follows a χ^2 distribution with four degrees of freedom in the absence of a signal, and a non-central χ^2 distribution (again with 4 degrees of freedom) when a signal is present. See, for example, [40] for more details. Furthermore, ρ_{coh}^2 is now a function of only the waveform components h_μ and no longer the \mathcal{A}^μ parameters. Thus four of the original seven waveform parameters have been analytically maximized, leaving three to be searched over.

Calculating the maximized likelihood, as well as estimating the parameters $\hat{\mathcal{A}}^\mu$ requires an inversion of the matrix $\mathcal{M}_{\mu\nu}$. CBC signals will spend a large number of cycles in the sensitive band of the detector and consequently the 0 and $\frac{\pi}{2}$ phases will be (close to) orthogonal. Since the frequency evolves slowly, the amplitudes of the two phases will be close to equal,⁴ i.e.

$$(h_0^X|h_{\frac{\pi}{2}}^X) \approx 0 \quad (2.27)$$

$$(h_{\frac{\pi}{2}}^X|h_{\frac{\pi}{2}}^X) \approx (h_0^X|h_0^X) =: (\sigma^X)^2. \quad (2.28)$$

Therefore, the matrix \mathcal{M} simplifies to

$$\mathcal{M}_{\mu\nu} = \begin{pmatrix} A & C & 0 & 0 \\ C & B & 0 & 0 \\ 0 & 0 & A & C \\ 0 & 0 & C & B \end{pmatrix} \quad (2.29)$$

where

$$\begin{aligned} A &= \sum_X (\sigma^X F_+^X)^2 \\ B &= \sum_X (\sigma^X F_X^X)^2 \\ C &= \sum_X (\sigma^X F_+^X)(\sigma^X F_X^X). \end{aligned} \quad (2.30)$$

In this form the detection statistic is almost identical to the \mathcal{F} -statistic for detecting rotating neutron stars, as described in [33], in the case where the neutron star has a small wobble angle.

Dominant Polarization

Since we have included a polarization angle in both the transformation between geocentric and radiation frame (χ) and between radiation and source frame (ψ), we have

⁴ Indeed, several CBC waveforms are generated directly in the frequency domain [41], making these equalities exact.

the freedom to specify one of these without placing any physical restriction on the signal. The coherent SNR is further simplified by introducing a dominant polarization frame which renders $\mathcal{M}_{\mu\nu}$ diagonal.

Under a rotation of the radiation frame by an angle χ^{DP} , the detector response functions transform as

$$\begin{aligned} F_+^X &\rightarrow F_+^{\text{DP},X} = F_+^X \cos 2\chi^{\text{DP}} + F_\times^X \sin 2\chi^{\text{DP}} \\ F_\times^X &\rightarrow F_\times^{\text{DP},X} = -F_+^X \sin 2\chi^{\text{DP}} + F_\times^X \cos 2\chi^{\text{DP}}. \end{aligned} \quad (2.31)$$

The rotation through χ^{DP} will have an identical effect on all detectors. Thus, there exists a polarization angle χ^{DP} which satisfies

$$C^{\text{DP}} = \sum_X (\sigma^X F_+^{\text{DP},X})(\sigma^X F_\times^{\text{DP},X}) = 0. \quad (2.32)$$

This can be solved to give χ^{DP} as

$$\tan 4\chi^{\text{DP}} = \frac{2 \sum_X (\sigma^X F_+^X)(\sigma^X F_\times^X)}{\sum_X [(\sigma^X F_+^X)^2 - (\sigma^X F_\times^X)^2]}. \quad (2.33)$$

This choice serves to diagonalize the matrix \mathcal{M} . To uniquely determine χ^{DP} , we impose an additional requirement that the network be more sensitive to the $+$ polarization than to the \times polarization. The value of χ^{DP} is a function of the detector network, the source location and waveform; in particular it depends upon $F_{+,X}^X$ and σ^X . From now on, we assume that we are working in the dominant polarization frame and drop the DP superscript from our expressions.

The concept of the dominant polarization frame has been introduced previously in un-modelled burst searches [42–44]. While the idea is very similar, the actual implementation is somewhat different.

In the case that both A and B are non-zero, i.e. that the detector has some sensitivity to both polarizations, the coherent SNR can be written, in the dominant polarization, as

$$\begin{aligned} \rho_{\text{coh}}^2 &= \frac{(\mathbf{s}|\mathbf{F}_+ \mathbf{h}_0)^2 + (\mathbf{s}|\mathbf{F}_+ \mathbf{h}_{\frac{\pi}{2}})^2}{(\mathbf{F}_+ \mathbf{h}_0 | \mathbf{F}_+ \mathbf{h}_0)} + \\ &\quad \frac{(\mathbf{s}|\mathbf{F}_\times \mathbf{h}_0)^2 + (\mathbf{s}|\mathbf{F}_\times \mathbf{h}_{\frac{\pi}{2}})^2}{(\mathbf{F}_\times \mathbf{h}_0 | \mathbf{F}_\times \mathbf{h}_0)}. \end{aligned} \quad (2.34)$$

The coherent SNR can then be seen to arise as the quadrature sum of the power in the two phases of the waveform (0 and $\frac{\pi}{2}$) in the two gravitational wave polarizations (+ and \times).

Network Degeneracy

In many cases, a detector network is much more sensitive to one gravitational wave polarization than the other. In the extreme limit (e.g. co-located and co-aligned detectors such as those at the Hanford site) the network is entirely insensitive to the second polarization. In the

dominant polarization frame, the network becomes degenerate as $B \rightarrow 0$ or equivalently

$$\sum_X (\sigma^X F_\times^X)^2 \rightarrow 0. \quad (2.35)$$

Thus the network will only be degenerate if $F_\times^X = 0$ for all detectors X. If the network is degenerate then it is easy to see that the detection statistic will be degenerate as well. In this case it is logical to remove the \times terms from the detection statistic reducing it to

$$\rho_{\text{coh}}^2 = \frac{(\mathbf{s}|\mathbf{F}_+ \mathbf{h}_0)^2 + (\mathbf{s}|\mathbf{F}_+ \mathbf{h}_{\frac{\pi}{2}})^2}{(\mathbf{F}_+ \mathbf{h}_0 | \mathbf{F}_+ \mathbf{h}_0)}, \quad (2.36)$$

which is χ^2 distributed with two degrees of freedom.

In this formalism the coherent SNR changes abruptly from (2.36) to (2.34). If there is any sensitivity, no matter how small, to the \times polarization, there is an entirely different detection statistic. This arises due to maximization over the \mathcal{A}^μ parameters, allowing them to take any value. Thus, even though a network may have very little sensitivity to the \times polarization, and consequently there be little chance of observing the waveform in the \times polarization, this is not taken into account in the derivation. A possible modification is to place an astrophysical prior on the parameters (D, ι, ψ, ϕ_0) and propagate this to the distribution of the \mathcal{A}^μ [45]. This would provide a smooth transition from the degenerate to non-degenerate search.

C. Comparison with Coincident Search

The single detector search is a special case of the degenerate network (2.36) and can be written as

$$\rho_X^2 = \frac{(s^X | h_0)^2 + (s^X | h_{\frac{\pi}{2}})^2}{(\sigma^X)^2}. \quad (2.37)$$

A coincidence search requires a signal to be observed in two or more detectors, without requiring consistency of the measured waveform amplitudes in the different detectors. In many cases, coincidence searches have made use of different template banks in the different detectors [4, 16, 27] and required coincidence between the recovered mass parameters [46]. A comparison with the coherent analysis discussed above is facilitated if we consider a coincident search where an identical template is used in all detectors, as was done in an analysis of early LIGO data [47]. In this case, the multi-detector coincident SNR is given by

$$\rho_{\text{coinc}}^2 = \sum_X \rho_X^2 = \sum_X \frac{(s^X | h_0)^2 + (s^X | h_{\frac{\pi}{2}})^2}{(\sigma^X)^2}. \quad (2.38)$$

This is not immediately comparable to the coherent SNR given in (2.34). However, both can be re-cast into similar forms by writing the coincident SNR as

$$\rho_{\text{coinc}}^2 = \sum_{X,Y} \sum_{i=0,\frac{\pi}{2}} \left(s^X \left| \frac{h_i}{\sigma^X} \right. \right) [\delta^{XY}] \left(s^Y \left| \frac{h_i}{\sigma^Y} \right. \right) \quad (2.39)$$

Similarly, the coherent SNR can be written as

$$\rho_{\text{coh}}^2 = \sum_{X,Y} \sum_{i=0,\frac{\pi}{2}} \left(s^X \Big| \frac{h_i}{\sigma^X} \right) [f_+^X f_+^Y + f_\times^X f_\times^Y] \left(s^Y \Big| \frac{h_i}{\sigma^Y} \right) \quad (2.40)$$

where we have defined the orthogonal unit vectors (in detector space) f_+^X, f_\times^X as

$$f_{+, \times}^X = \frac{\sigma^X F_{+, \times}^X}{\sqrt{\sum_Y (\sigma^Y F_{+, \times}^Y)^2}}. \quad (2.41)$$

The SNR of the coincident search (2.39) is simply the sum of all power consistent with the template waveform in each detector. The coherent SNR (2.40) makes use of the fact that gravitational waves have only two polarizations to restrict the accumulated SNR to the physical subspace spanned by f^+ and f^\times . For a signal, the power will lie entirely in this subspace, while noise in the detectors will contribute to all components of the coincident SNR. Thus, the coherent analysis obtains precisely the same signal SNR but reduces the noise background. Specifically, the coherent SNR acquires contributions from four noise degrees of freedom, while the coincident SNR has $2N$ noise degrees of freedom, where N indicates the number of active detectors. For a non-degenerate two detector network, the coincident and coherent SNRs are equal as in this case $f_+^X f_+^Y + f_\times^X f_\times^Y = \delta^{XY}$. In the case where a network is sensitive to only one polarization, the coherent SNR is constructed solely from the f_+^X direction and coherent SNR is χ^2 distributed with 2 degrees of freedom.

Finally, we note that restricting to the coherent SNR can help to separate transients from gravitational wave signals as those transients which do not contribute power to the signal space will be ignored. However, many noise transients will contribute to the coherent SNR and more active methods of removing them are required. These methods are the focus of sections III and IV.

D. Synthetic + and \times detectors

In the dominant polarization the coherent SNR is comprised of separate $+$ and \times components, with no cross terms. We can go one step further and interpret the coherent SNR as arising from two synthetic detectors, one sensitive to only the $+$ polarization and one sensitive to only the \times polarization. These synthetic detectors are most easily formed by combining the “overwhitened” data streams o^X from the various detectors, where

$$o^X(f) = \frac{s^X(f)}{S_h^X(f)}. \quad (2.42)$$

The overwhitened synthetic data streams are simply

$$o_{+, \times}(f) = \sum F_{+, \times}^X o^X(f); \quad (2.43)$$

and the power spectra for these overwhitened data streams are

$$S_{+, \times} = \left(\sum_X \frac{(F_{+, \times}^X)^2}{S_h^X(f)} \right)^{-1}. \quad (2.44)$$

Using this, the un-whitened synthetic data streams are given as⁵

$$s_{+, \times}(f) = \sum_X \frac{F_{+, \times}^X s^X(f)}{S_h^X(f)} \left(\sum_Y \frac{(F_{+, \times}^Y)^2}{S_h^Y(f)} \right)^{-1}. \quad (2.45)$$

In terms of these synthetic detectors the detection statistic becomes

$$\rho_{\text{coh}}^2 = \frac{(s_+ | h_0)_+^2 + (s_+ | h_{\frac{\pi}{2}})_+^2}{(h_0 | h_0)_+} + \frac{(s_\times | h_0)_\times^2 + (s_\times | h_{\frac{\pi}{2}})_\times^2}{(h_0 | h_0)_\times}, \quad (2.46)$$

where the subscripts $+, \times$ on the inner products denote the fact that the power spectrum of the synthetic detectors is used in their evaluation.

III. SIGNAL CONSISTENCY BETWEEN DETECTORS

As discussed in the introduction, due to the presence of non-Gaussian noise transients, it is essential to make use of signal consistency requirements within search algorithms to distinguish glitches from gravitational wave signals.

Multi-detector analyses have made good use of signal consistency between detectors (see e.g. [44]). A particularly powerful test is the use of a “null stream” [26] which, by construction, contains no gravitational wave signal. Many noise transients will contribute power to the null stream and can therefore be eliminated as candidate events. In addition, requiring that the gravitational wave signal is recovered consistently between detectors can eliminate other noise transients, in our case this is equivalent to imposing restrictions on the recovered values of the parameters, $\hat{\mathcal{A}}^\mu$. These two methods will be considered in turn. For matched filtering searches, requiring consistency between the observed signal and template waveform has also proven very powerful [24]. A full description of waveform consistency tests is presented in the next section.

A. Null Stream Consistency

The gravitational waveform consists of two polarizations. Thus for networks comprising three or more detectors it is possible to construct one or more null data

⁵ There is some ambiguity in fixing the overall normalization of the synthetic detectors. We require that our synthetic detectors have the same sensitivity to the two polarizations as the original network did by requiring $(h_0^{+, \times} | h_0^{+, \times})_{+, \times} = \sum_X (F_{+, \times}^X \sigma^X)^2$.

streams which contain no gravitational wave signal [26]. In the context of a coherent search for CBC signals, the null consistency tests arise quite naturally. In section II C, we noted that the coherent SNR can be thought of as a projection of the coincident multi-detector SNR onto a four dimensional signal subspace. The remaining dimensions in the coincident search do not contain any gravitational wave signal, but will be subject to both Gaussian and non-Gaussian noise. Thus, we can define the null SNR as

$$\begin{aligned} \rho_N^2 &= \rho_{\text{coinc}}^2 - \rho_{\text{coh}}^2 \\ &= \sum_{X,Y} \sum_{i=0,\frac{\pi}{2}} \left(s^X \left| \frac{h_i}{\sigma^X} \right. \right) [N^{XY}] \left(s^Y \left| \frac{h_i}{\sigma^Y} \right. \right), \end{aligned} \quad (3.1)$$

where

$$N^{XY} = \delta^{XY} - f_+^X f_+^Y - f_\times^X f_\times^Y. \quad (3.2)$$

A gravitational wave signal matching the template h will provide no contribution to the null SNR, so we expect that, for signals, this statistic will be χ^2 distributed with $(2N - 4)$ degrees of freedom. A noise transient that is incoherent across the data streams, may give a large coherent SNR, but it is likely to also give a large null SNR. Thus requiring a *small* null SNR will prove effective at distinguishing incoherent noise transients from real gravitational wave signals. Since the definition of the null SNR (3.1) makes use of the template waveform, gravitational waveforms which do not match the template h can contribute to the null SNR.

We can go one step further and introduce synthetic null detectors in analogy with the synthetic + and \times detectors. For concreteness, we describe the three detector case, but this can be extended in a straightforward manner to larger networks. To do so, we introduce the null direction

$$n^X = \epsilon^{XYZ} f_+^Y f_\times^Z. \quad (3.3)$$

such that $N^{XY} = n^X n^Y$. Then, the over-whitened synthetic null detector is

$$o_N(f) = \sum \frac{n^X}{\sigma^X} o^X(f). \quad (3.4)$$

The power spectrum of the null stream is⁶

$$S_N(f) = \left(\sum_X \frac{(n^X)^2}{(\sigma^X)^2 S_h^X(f)} \right)^{-1} \quad (3.5)$$

and the un-whitened null stream is

$$s_N(f) = \left(\sum_X \frac{n^X s^X(f)}{\sigma^X S_h^X(f)} \right) \cdot S_N(f). \quad (3.6)$$

Finally, the null SNR can be written as

$$\rho_N^2 = \frac{(s_N|h_0)_N^2 + (s_N|h_{\frac{\pi}{2}})_N^2}{(h_0|h_0)_N}. \quad (3.7)$$

The null SNR described above differs from the multi-detector null stream formalism introduced in [26] and used by several other authors. A null stream is constructed to be a data stream which contains no contribution from the h_+ and h_\times gravitational waveforms, regardless of the details of the waveform. To provide a concrete comparison between the null stream and null SNR, we restrict attention to a three detector network. The null stream is explicitly constructed as

$$s_{\text{Null}}(f) = \epsilon_{XYZ} F_+^X F_\times^Y s^Z(f). \quad (3.8)$$

By comparing the null stream in (3.8) with the synthetic null detector (3.6), it is clear that these will generically differ. To get an insight into the differences, consider a network with two co-located detectors A and B , with power spectra $S_h^A(f)$ and $S_h^B(f)$ respectively, and a third detector C which is sensitive to the other polarization of gravitational waves. For this network, the null stream will be a combination of only the A and B detector data. The power spectrum of the null stream is

$$S_{\text{Null}}(f) = S^A(f) + S^B(f). \quad (3.9)$$

while for the synthetic null detector, it is

$$\frac{1}{S_N(f)} = \frac{1}{(\sigma^A)^2 S^A(f)} + \frac{1}{(\sigma^B)^2 S^B(f)}. \quad (3.10)$$

Thus, if the power spectra of detectors A and B are identical, then the two null streams are also identical. In the extreme case that the sensitivity bands of the two detectors do not overlap at all, then there is no null stream ($S_{\text{Null}} \rightarrow \infty$). However, the null SNR need not vanish and is similar to a two bin version of the χ^2 test described in section IV D. Thus, it is possible to construct scenarios in which these two null stream formulations differ significantly.

For the most part, the power spectra of the ground based detectors are rather comparable. So, in general there will not be a significant difference between these two forms. There are advantages to both methods. The null stream is designed to cancel all gravitational wave signals from the data, thus making it more robust when the signal is not well known. However, by making use of the template signal, there are instances in which the null SNR provides a more powerful consistency test. Furthermore, it has a computational benefit in that it does not require the production of a null stream — all manipulations are performed on the single detector SNR data

⁶ In this case, there is a normalization ambiguity. For the synthetic plus and cross streams, it was natural to require that the synthetic detectors have the same sensitivities as the original network. For the null stream this is not feasible as the network has zero sensitivity to a signal in the null stream, so we normalize such that $(h_0|h_0)_N = 1$.

streams which are subsequently separated into coherent and null components. In practice we have found very little difference in performance, and choose to compute the null SNR (3.1) for computational simplicity.

Finally, we note that both null stream formalisms will perform optimally only if the three detectors have similar sensitivities. In the case where one detector is significantly less sensitive than the others, the null stream will generally tend to the data of that less sensitive detector. Also, the null formalisms described here will only completely cancel a gravitational wave signal provided that the calibration of the data streams is accurate, any error in calibration will lead to a signal surviving in the null stream data.

B. Amplitude Consistency

The four amplitude parameters \mathcal{A}^i , encoding the distance to and orientation of the binary system, can take any values. Indeed, any set of \mathcal{A}^i corresponds to unique values of the distance, inclination angle, coalescence phase and polarization angle, up to symmetries of the system. However, some of these values will be significantly more likely to occur astrophysically than others. For example, the number of binary coalescence events is expected to be approximately proportional to star formation rate [11] and consequently should be roughly uniform in volume. Thus, events are more likely to occur at a greater distance. Similarly, the gravitational wave amplitude, at a fixed distance, is greater for face on signals than edge on ones, as is clear from (2.5). Thus, approximately face on signals at a large distance are more likely signals than nearby, edge on ones.

The distribution of noise events will follow its own characteristic distribution. For Gaussian noise, this distribution can be evaluated and the signal and noise distributions incorporated into the ranking statistic [45]. Non-stationarities in the data will again produce a different distribution of amplitudes. Specifically, the majority of transients are caused by a disturbance or glitch in a single detector with little or no signal in the other detectors. For networks with three or more detectors, this will typically be inconsistent with a coherent signal across the network, leading to a large value of the null SNR. In certain scenarios, most notably for two detector networks, there will be a consistent set of values for the \mathcal{A}^i . However, these values carry the characteristic signature of a glitch. Specifically, the SNR contributions will typically be consistent with a nearby, close to edge on system ($A_x \approx 0$), with a very specific orientation to provide essentially no response in all but one detector. Thus, the glitch distribution of the \mathcal{A}^i parameters, will be significantly different from the distribution expected for gravitational wave signals. In the remainder of this section, we explore the possibility of making use of the extracted \mathcal{A}^i parameters to distinguish between glitches and signals. Unlike the null stream, amplitude consistency tests are available for

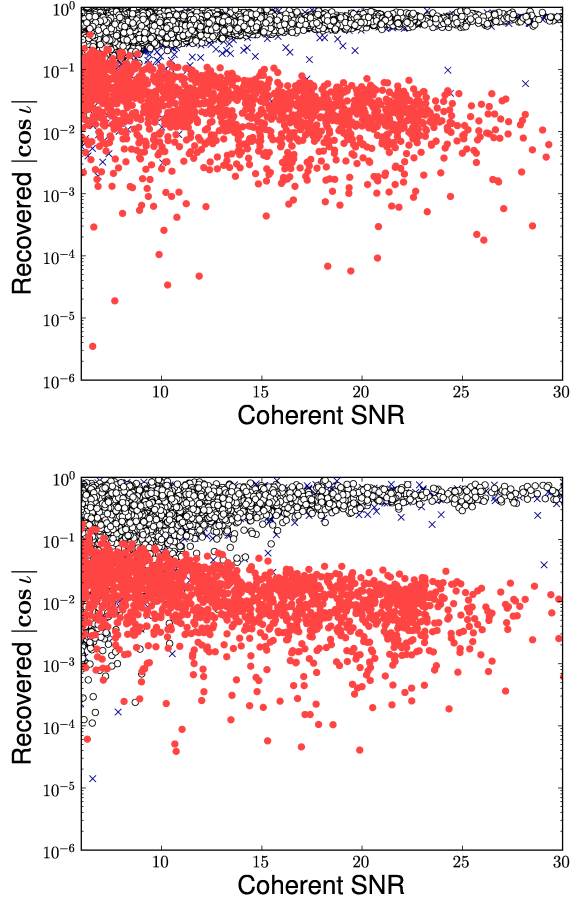


FIG. 1. The distribution of the recovered inclination angle plotted against coherent SNR for optimally oriented signals (unfilled circles), uniformly distributed orientations (blue crosses) and simulated glitches (red circles). The top figure shows a network configuration where we are equally sensitive to both gravitational wave polarizations. The bottom figure shows a configuration where we are 5 times more sensitive to the + polarization than to the \times .

two detector networks. They should be especially useful in the case of the two 4km LIGO instruments, which have similar sensitivities to the majority of points on the sky.

We have argued that the majority of gravitational wave signals will originate from (close to) face on binaries while the majority of noise transients will mimic (close to) edge on binaries. The recovered value of the inclination angle ι should then serve to separate signals from noise. To investigate this, we simulated a large number of simulated CBC signals and a large number of noise glitches; added Gaussian noise and plotted the recovered inclination angle in Figure 1. The glitches were generated as events with a large SNR in one detector coincident with Gaussian noise in a second detector. The signals were separated into two groups: the first with only face on binaries ($|\cos \iota| = 1$) and the second a uniform distribution over the two sphere (uniform in $\cos \iota$ and ψ) of the binary ori-

entation. In both cases, they were distributed uniformly in volume and orbital phase. We also consider different network configurations, both containing two equally sensitive detectors. In the first case one detector is sensitive to $+$ and the other to \times polarization ; in the second case both detectors have strong and equal sensitivity to the $+$ polarization and weak but opposite sensitivity to the \times polarization — rather typical for the Hanford, Livingston network. For both sets of signals and choices of network, there is a clear distinction between signal and glitch distribution. However, there is a clear downwards bias on the recovered values of ι . This can be understood by looking at the expressions for A_+ and A_\times . For face on binaries, these will be equal but, in the presence of noise, A_\times will be reconstructed to be somewhat smaller than A_+ . A relative difference of only 5% leads to a recovered inclination of 45° , so even for loud signals there can be large discrepancy between the actual and recovered inclination angle.

Despite the difference in distribution between signal and noise, there is also a significant overlap of the populations at low SNRs. Consequently, any threshold imposed on the recovered inclination angle is liable to either reject a fraction of signals or pass a fraction of glitches. It is, however, quite possible that knowledge of these expected distributions could be folded into the detection statistic in a Bayesian manner.

We have found that using the observed SNR in the individual instruments to be a more effective discriminator of signal and noise. To demonstrate the efficacy of such an approach, in Figure 2 we plot the single detector SNR as a function of the coherent SNR for the same population of glitches and the two classes of signals (face on and uniformly distributed orientation) described above. The glitches fall into two groups depending upon which detector suffered the glitch. Since our model detectors are equally sensitive, then on average one expects each detector to accrue $1/\sqrt{2}$ of the coherent SNR. Even allowing for non-optimally oriented signals and the addition of Gaussian noise, the signals follow this expectation. Only a small number of signals are found with SNRs inconsistent with the expected values, these are ones that have very specific orientations. Overall, the signal and glitch populations are very well separated, at least until the coherent SNR becomes rather small.

The most effective strategy we have found is to require that all events have an SNR above 4 in the two most sensitive detectors in the network. The cut is illustrated in Figure 2. This strategy removes the majority of glitch signals while having a negligible effect on the signal population at large SNR. For lower SNR the signals which are lost due to this cut would be unlikely to be detection candidates as Gaussian noise alone produces similar events.

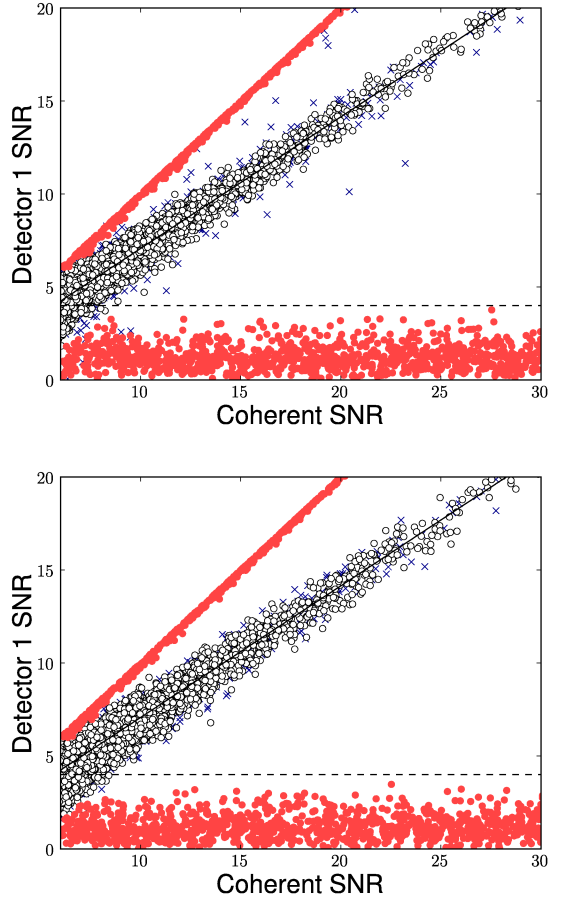


FIG. 2. The distribution of single detector SNR plotted against coherent SNR for optimally oriented signals (unfilled circles), uniformly oriented signals (blue crosses) and glitches (red circles). The top figure shows a two equally sensitive detector network configuration where one detector sees only the $+$ polarization and the second detector sees only the \times polarization. The bottom figure shows a two detector network configuration where both detectors have strong and equal sensitivity to the $+$ polarization and weak but opposite sensitivity to the \times polarization. This is meant to emulate a typical instance for the Hanford, Livingston network. The diagonal solid black line shows the expected SNR for the optimally oriented signals. The horizontal dashed black line indicates an SNR of 4.

IV. COHERENT χ^2 TESTS

Data from gravitational wave detectors contain numerous non-stationarities due to both instrumental and environmental causes. These non-stationarities, or glitches, typically do not match well with the CBC waveform. However, they often contain enough power that, even though the match with the template is poor, a large SNR is observed. In the previous section, we have seen how the use of various coherent consistency tests can mitigate this problem. Additionally, a number of other signal consistency tests have been implemented [24, 25] and used

in searches for CBC signals [4, 27, 28]. These tests are all designed to eliminate glitches which have a different signal morphology than the template waveform. This is essentially done by testing whether the detector data orthogonal to the signal is well described as Gaussian and stationary — for a glitch, there will be residual power which does not match the template waveform. These tests are commonly known as “ χ^2 tests” as they construct a statistic which is χ^2 distributed in the presence of Gaussian noise plus a signal matching the template waveform. If the data contains a glitch, the χ^2 statistic will generally have a large value, thereby allowing for differentiation of signal from non-stationary noise. In this section, we briefly review the general formulation of χ^2 tests before presenting a detailed description of three such tests which have been implemented for the coherent search described in section II.

A. A general framework for χ^2 tests

Consider the data from a gravitational wave detector at a time t which has produced a large SNR when filtered against a template $h(t)$. Generically, the data $s(t)$ can be decomposed as

$$s(t) = n(t) + Ah(t) + Bg(t) \quad (4.1)$$

where $n(t)$ represents a Gaussian noise component, $h(t)$ is the template waveform, $g(t)$ is an additional non-Gaussian noise contribution to the data stream and A and B are amplitude factors. The glitch contribution $g(t)$ is taken to be the power orthogonal to $h(t)$ and both $g(t)$ and $h(t)$ are normalized, so that

$$(g|g) = 1, (h|h) = 1, (g|h) = 0. \quad (4.2)$$

In order to construct a χ^2 test, we must introduce an additional set of waveforms T^i . These waveforms are required to be orthonormal and orthogonal to h ,

$$(h|T^i) = 0, (T^i|T^j) = \delta^{ij}. \quad (4.3)$$

Furthermore, for the χ^2 test to be effective, the T^i must have a good overlap with the glitch waveform $g(t)$.

The χ^2 discriminator is constructed as

$$\chi^2 = \sum_{i=1}^N (T^i|s)^2. \quad (4.4)$$

When the data comprises only signal plus Gaussian noise, i.e. $B = 0$ in equation (4.1),

$$\chi^2 = \sum_{i=1}^N (T^i|n)^2. \quad (4.5)$$

and the statistic is the sum of squares of independent Gaussian variables with zero mean and unit variance.

Thus the test is χ^2 distributed with N degrees of freedom, with a mean and variance of

$$\langle \chi^2 \rangle = N, \quad \text{Var}(\chi^2) = 2N. \quad (4.6)$$

This is true for *any* set of waveforms T^i given the above assumptions.

In the case where the data are not an exact match to the signal, we take both A and B non-zero, i.e. any signal or glitch can be decomposed into a part $Ah(t)$ proportional to the template under consideration plus a second orthogonal contribution $Bg(t)$. Clearly, for different glitches, the waveform $g(t)$ as well as the amplitude factor B will be different. In this case the χ^2 test takes the form

$$\chi^2 = \sum_{i=1}^N [(T^i|n)^2 + 2B(T^i|n)(T^i|g) + B^2(T^i|g)^2]. \quad (4.7)$$

This has a mean

$$\langle \chi^2 \rangle = N + B^2 \sum_i (T^i|g)^2 \quad (4.8)$$

and a variance

$$\text{Var}(\chi^2) = 2N + 4B^2 \sum_i (T^i|g)^2. \quad (4.9)$$

The χ^2 test is distributed as a non-central χ^2 distribution with N degrees of freedom and a non-centrality parameter [24]

$$\lambda = B^2 \sum_{i=1}^N (T^i|g)^2. \quad (4.10)$$

The challenge in constructing a χ^2 test is to select the basis waveforms T^i such they have large overlaps with the observed glitches in the data. If this is done successfully, then any glitch producing a large SNR will also give a large value of χ^2 , inconsistent with a signal in Gaussian noise.

In many cases, there is some uncertainty in the template waveform. For example, the post-Newtonian (PN) expansion used in generating CBC waveforms is truncated at a finite (typically 3 or 3.5 PN [48]) order and there will be differences between this analytically calculated waveform and the one provided by nature. There are similar uncertainties in waveforms obtained from numerical relativity simulations [49]. Additionally, to search the full parameter space of coalescing binaries, a discrete template bank is used which allows for some mismatch between the templates and any potential signal within the parameter space [37]. Normally the template bank is created so that the mismatch is no larger than 3% at any point in the parameter space. Finally, there are uncertainties in instrumental calibration [50] which will affect the match between signal and template.

We model these effects by parametrizing the signal as

$$H(t) = A(\sqrt{1 - \epsilon^2} h(t) + \epsilon m(t)), \quad (4.11)$$

where $m(t)$ is the component of H that is orthogonal to h [$(m|h) = 0$] and ϵ encodes the mismatch between signal and template in the sense that

$$1 - \frac{(H|h)}{\sqrt{(H|H)(h|h)}} = 1 - \sqrt{1 - \epsilon^2} \approx \epsilon. \quad (4.12)$$

In most cases, it is reasonable to assume a mismatch of less than 5%. The obvious counter-example is when searching for highly spinning systems using non-spinning waveforms, see e.g. [51, 52].

Since (4.11) is a special case of (4.1) it follows directly that the mean and variance of the χ^2 test in the presence of a mis-matched signal are

$$\begin{aligned} \langle \chi^2 \rangle &= N + A^2 \epsilon^2 \sum_{i=1}^N (T^i|m)^2 \\ \text{Var}(\chi^2) &= 2N + 4A^2 \epsilon^2 \sum_{i=1}^N (T^i|m)^2. \end{aligned} \quad (4.13)$$

Since the SNR of the signal is proportional to A , the expected χ^2 value for a mis-matched signal increases with the strength of the signal. However, for mismatched signals $\chi^2 \propto \epsilon^2 A^2$ while for glitches $\chi^2 \propto B^2$ and provided $\epsilon A \ll B$ the two can be separated. See [24] for a more detailed discussion.

When introducing the χ^2 test, we assumed that the T^i were orthonormal and orthogonal to the template waveform h . In practice, this can be difficult to guarantee. The signal consistency tests discussed in the remainder of this section are constructed from gravitational waveforms. If one picks a set of gravitational waveforms, t^i , there is no guarantee that they will be either orthonormal or orthogonal to h . We can, at least, construct waveforms which are orthogonal to h by introducing

$$T^i = \frac{t^i - (t^i|h)h}{\sqrt{1 - (t^i|h)^2}}. \quad (4.14)$$

While this ensures $(h|T^i) = 0$ it does not guarantee orthonormality of the T^i , $(T^i|T^j) = \delta^{ij}$. Thus this method will not produce a χ^2 distribution, and will instead form a generalized χ^2 distribution. The mean of the distribution remains N but the variance is increased,

$$\text{Var}(\chi^2) = 2N + 2 \sum_{i \neq j} (T^i|T^j)^2. \quad (4.15)$$

It has been found, however, that this does not present a significant obstacle to using these tests, especially as the thresholds are tuned empirically [53].

Multi-detector χ^2 tests

In section II, we derived a coherent multi-detector search for coalescing binaries. The search involves filtering four waveform components h_μ against the multi-detector data stream. Our initial discussion of χ^2 tests was limited to the description of a single phase template waveform h and test waveforms T^i . The extension to a two phase waveform has been described previously [24] and here we extend that to a four component waveform across multiple detectors, as is appropriate for this search. We begin by noting that the four waveform components h_μ are orthogonal in the dominant polarization basis. They are, however, not generally normalized, as

$$(h_\mu|h_\nu) = \mathcal{M}_{\mu\nu} = \text{diag}(A, B, A, B), \quad (4.16)$$

where A and B are defined in (2.30). Thus, we first normalize so that

$$(\hat{h}_\mu|\hat{h}_\nu) = \delta_{\mu\nu}. \quad (4.17)$$

To construct a network χ^2 test, we require a set of (4-component) normalized, test waveforms \hat{t}_μ^i . The components

$$T_\mu^i = \frac{\hat{t}_\mu^i - \sum_\nu (\hat{t}_\mu^i|\hat{h}_\nu)\hat{h}_\nu}{\sqrt{1 - \sum_\sigma (\hat{t}_\sigma^i|\hat{h}_\sigma)^2}}, \quad (4.18)$$

constructed to be orthogonal to h_μ , are used in the χ^2 test. Thus, the coherent, multi-detector χ^2 test is

$$\chi^2 = \sum_{\mu=1}^4 \sum_{i=1}^N (T_\mu^i|\mathbf{s})^2. \quad (4.19)$$

Provided the test waveforms are orthonormal, in the sense that

$$(T_\mu^i|T_\nu^j) = \delta^{ij}\delta_{\mu\nu}, \quad (4.20)$$

the distribution for a signal matching h_μ plus Gaussian noise will be χ^2 distributed with $4N$ degrees of freedom. As for the single phase filter, we cannot always guarantee (4.20) is satisfied, although it is relatively simple to ensure the four components of a given template are orthogonal. This means that the statistic will not, in general, be χ^2 distributed: The mean remains $4N$ but the variance increases to

$$\text{Var}(\chi^2) = 8N + 2 \sum_{i,j=1}^N \sum_{\mu,\nu=1}^4 [(T_\mu^i|T_\nu^j)^2 - \delta^{ij}\delta_{\mu\nu}]. \quad (4.21)$$

B. The coherent bank χ^2 test

The bank χ^2 test was designed to test the consistency of the observed SNR across different templates in the

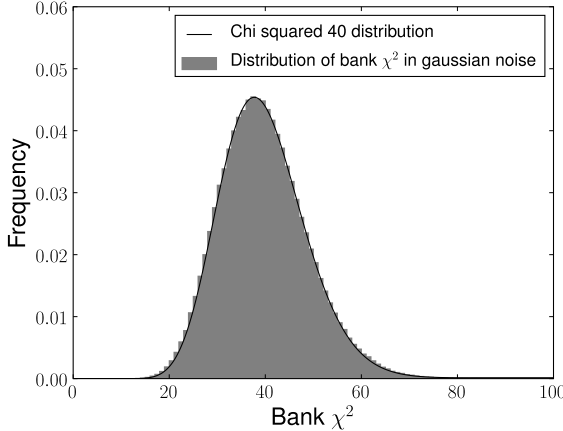


FIG. 3. The distribution of the bank χ^2 test for a single template h , with a bank of size 10. The plot shows the distribution of the bank veto calculated for every time sample in 128s of simulated Gaussian data (with no signal present). In the case that the ten bank templates are orthogonal, the expected distribution is χ^2 with 40 degrees of freedom (shown as the solid black line). As can be seen, the actual distribution follows the expected one closely.

bank at the time of a candidate signal. It was first described in [25] for the case of a single detector. A glitch will typically cause a high SNR in many templates across the bank, while a real signal will give a well prescribed distribution of SNR across the template bank.

The bank χ^2 makes use of other CBC templates as the waveforms t^i to construct the χ^2 test. These N templates are taken from different points across the mass space. In implementing the bank χ^2 , we choose a *fixed* set of template waveforms t^i which remain the same for every template h in the search template bank. The bank χ^2 statistic is then constructed following (4.18) and (4.19). The test is most effective when the set of T_μ^i is close to orthogonal [25] so we select templates which are well distributed across the mass space, ensuring the overlaps ($T_\mu^i | T_\nu^j$) are small for $i \neq j$. Figure 3 shows the distribution of the bank χ^2 for a single template filtered against Gaussian noise. The set of fixed bank waveforms consisted of ten waveforms distributed over the full mass parameter space. Using these waveforms, the deviation from a χ^2 distribution is negligible.

For the bank χ^2 to be effective, glitches in the data must have a good overlap with a reasonable fraction of the templates t^i . While, in general, it is difficult to predict the composition of glitches in the data, it seems reasonable to assume that glitches which produce a large SNR for the template h will also have a good overlap with other waveforms in the template space. Thus, the set of templates which is spread across the parameter space is suitable.

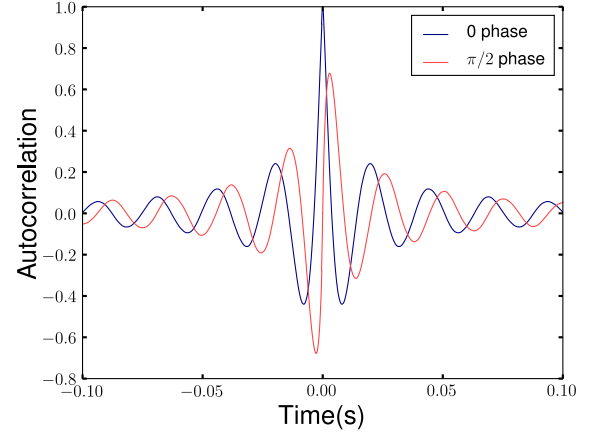


FIG. 4. The single detector auto-correlation of a gravitational wave inspiral signal from a 1.4,1.4 solar mass binary neutron star. Both phases of the waveform are shown.

C. The coherent autocorrelation χ^2 test

Filtering a gravitational wave template against data containing a matching signal produces a peak in the SNR at the time of the signal. Furthermore, there is a characteristic shape of this peak which depends upon the template waveform and also the noise power spectrum of the data. An example of this “autocorrelation” for a binary neutron star template is shown in Figure 4. A noise transient in the data will produce a peak in the SNR but it will typically lack the characteristic shape produced by a genuine CBC signal.

The “auto” χ^2 test was designed to test the consistency of the SNR peak [25]. It is a similar test to the bank χ^2 , but where the bank χ^2 investigates consistency in SNR across the mass space, the auto χ^2 tests for consistency of the SNR time series. The set of templates t^i are chosen to be the original template h with time shifts δt^i applied. The values of δt^i are all unique and chosen to be of the same time-scale as the auto-correlation of the template waveform (typically 0.1s or less) and the duration of non-stationarities in the data, which is similar.

In Figure 5, we show the distribution of the auto χ^2 for a single template waveform filtered in Gaussian data. For this result, forty waveforms t^i were used, equally spaced with a 1 ms spacing, and all with coalescence times prior to that of h . Thus, the auto χ^2 is testing the consistency of the SNR time series for 0.04 seconds prior to the SNR peak. The overlap ($t^i | t^j$) depends only upon the difference $\delta t^i - \delta t^j$ and Figure 4 shows clearly that a significant fraction of the overlaps are far from zero. Consequently, the auto χ^2 test has a distribution with a large deviation from a χ^2 distribution with $4N$ degrees of freedom.

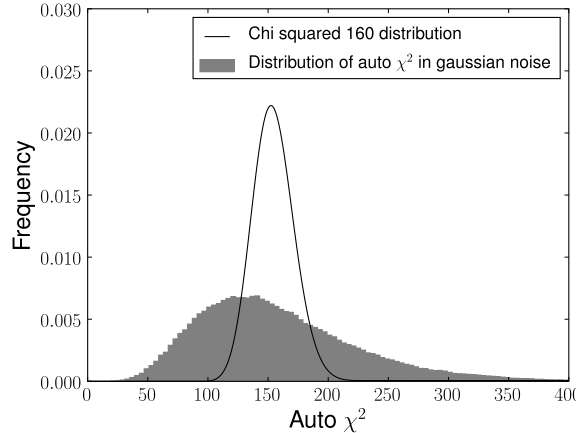


FIG. 5. The distribution of the auto χ^2 test for a single template h , generated with 40 time shifted templates, with shifts between 0.001 and 0.04 seconds. The plot shows the distribution of the auto veto calculated for every time sample in 128s of simulated Gaussian data (with no signal present). In the case that the forty time shifted templates are orthogonal, the expected distribution is χ^2 with 160 degrees of freedom (shown in black). As can be seen, the actual distribution differs significantly from this due to the non-orthogonality of the t^i waveforms.

D. The coherent χ^2 test

The “standard” χ^2 test originally proposed in [24] has been used as a discriminator in many gravitational wave searches for CBCs. Given the template waveforms and the detector sensitivity, it is possible to predict the accumulation of SNR as a function of frequency. By calculating the observed SNR contribution from a number of frequency bins, and comparing to the predicted value, one can construct a χ^2 consistency test.

Formally, given a template h which produced a candidate signal with an SNR of ρ , calculate N non-overlapping frequency windows such that the expected SNR is ρ/N in each. Then, calculate the actual SNR ρ^i in each of these frequency bins and compare with the expected value by calculating

$$\chi^2 = N \sum_i^N (\rho^i - \rho/N)^2. \quad (4.22)$$

For a gravitational wave signal matching the template h plus Gaussian noise, this statistic will be χ^2 distributed with $N-1$ degrees of freedom. Written in the form (4.22) it appears different from the general case we discussed earlier. In [24] it was shown that it can be re-expressed in the form (4.4).

This χ^2 test can be extended to coherent, multi-detector searches. Indeed, in [54], the construction was applied to a coherent search for continuous gravitational waves. Here, we present the extension to a coherent CBC

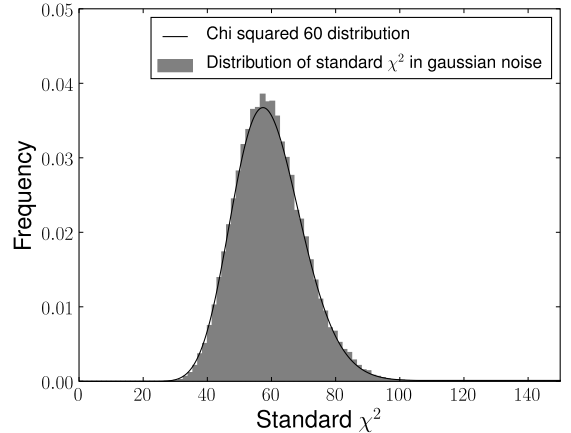


FIG. 6. The distribution of the χ^2 test for a single template h , split into 16 non-overlapping frequency bins. The plot shows the distribution of the χ^2 test calculated for every time sample in 128s of simulated Gaussian data (with no signal present). The observed distribution of values shows (shown in grey) is an excellent match with the expected χ^2 distribution with sixty degrees of freedom (shown in black).

search. First, define

$$\rho_\mu^i = \frac{(\mathbf{s}|\mathbf{h}_\mu^i)}{\sqrt{(\mathbf{h}_\mu|\mathbf{h}_\mu)}} \quad (4.23)$$

to be the SNR contribution in the i th frequency bin to the SNR.⁷ The coherent χ^2 statistic is then constructed as

$$\chi^2 = N \sum_{i=1}^N \sum_{\mu=1}^4 (\rho_\mu^i - \rho_\mu/N)^2. \quad (4.24)$$

As all the components are orthogonal it is easy to see that this statistic will be exactly χ^2 distributed with $4N-4$ degrees of freedom. One can interpret this as the sum of the single detector χ^2 values for the h_0 and $h_{\frac{\pi}{2}}$ waveforms in the synthetic + and \times detectors. Figure 6 shows the distribution of the “standard” χ^2 , using 16 frequency bins. The distribution matches the expected χ^2 with 60 degrees of freedom.

An alternative approach to applying the χ^2 test to a coherent search was proposed in [29]. This approach involves calculating the χ^2 values for each of the active detectors and using these values to veto glitches.

⁷ Strictly speaking the frequency bins for the F_+ and F_\times components will be different because, as we have noted in equation (2.44), the PSDs for the synthetic + and \times detectors are not equal. However, usually the difference between the two is small enough that it can be safely ignored to avoid computing twice the number of filters. Alternatively, in [24] a method was presented for calculating the standard χ^2 test using unequal frequency bins, that method could easily be incorporated into a coherent search.

V. IMPLEMENTATION AND PERFORMANCE OF A COHERENT SEARCH

In the previous sections we have presented a method for detecting gravitational waves from CBCs in a network of detectors. The coherent SNR described in II is ideal for distinguishing signals in Gaussian data and, in sections III and IV, we have introduced a number of strategies for discriminating between signal and noise in non-Gaussian, non-stationary data. Here, we describe an implementation of the targeted, coherent search for gravitational waves from CBC. In addition, we demonstrate its efficacy by performing test analyses of simulated data and real data taken from S4.

A. Implementation of a coherent triggered search for CBCs

Here, we describe the main steps by which the algorithms described in sections II, III and IV have been implemented. The analysis is available in the LIGO Scientific Collaboration Applications Library (LAL) suite [55], and makes use of a large number of tools and methods previously implemented in that library.

1. Analysis setup

A targeted, coincident search for gravitational waves from CBC associated to GRBs has been implemented, and used in a search of S5 and VSR1 data [16]. The coherent search pipeline uses many of the same definitions, and much of the same architecture to determine the analysis details. Specifically, “onsource” time is $[-5, +1]$ seconds around the reported time of the GRB; this is when a gravitational wave signal would be expected [20, 56]. The noise background is estimated using 1,944 seconds of “offsource” data split into 324 trials of 6 second length each. These are used to calculate the significance of any event occurring in the onsource. As in Ref. [16] we impose a 48s buffer zone between the onsource and offsource regions. To obtain an accurate estimate of the detectors’ power spectra, we only analyse data from a detector if it has taken at least 2190s of continuous data around the time of the GRB. Modulo this restriction, the coherent analysis is designed to make use of data from all detectors that were on at the time of the GRB.

2. Template bank generation

The problem of placing a template bank for a single detector has been extensively studied [37, 57–59]. However, less thought has been given to the problem of placing an appropriate bank for a coherent analysis. Our current method is to use a template bank generated for one of the detectors in the network. In the results presented later,

we have made use of a bank generated with the initial LIGO design spectrum, with a maximum total mass of $40M_{\odot}$ and a minimum component mass of $1M_{\odot}$, these are the same values as used in [16]. This method enables us to demonstrate the efficiency of this coherent search it is not the optimal solution. A simple improvement would involve placing a template bank appropriate for the (maximally sensitive) synthetic + detector defined in equation (2.44). In many cases, a network is significantly more sensitive to one GW polarization and, in these cases, this template bank would perform well.

3. Coherent SNR and Null Streams

The data are first read in and conditioned using the methods and algorithms developed for the S4 search for post-merger ringdowns from CBCs [60, 61]. The data are downsampled to a frequency of 4096Hz and split into overlapping 256 second segments for analysis. The noise PSDs are calculated using the same method as in [60].

Each template of the bank is filtered against the data from each detector to generate the single detector filters ($s^X | h_{0, \frac{\pi}{2}}^X$) and sensitivities σ^X . The algorithms used are taken from the LAL FindChirp library [62], specifically those written to perform a search for spinning waveforms [52] using the physical template family (PTF) waveforms [63].⁸ The waveform templates are generated using the TaylorT4 post-Newtonian approximant [41]. The single detector filter outputs are shifted in time to account for the relative delays from the given GRB sky location. They are then combined to form the coherent and the null SNRs as described by (2.40) and (3.1). A “trigger” is recorded at any time the coherent SNR is greater than 6, and no louder event occurred in any template in the bank within 0.1 seconds.

4. Calculating the χ^2 tests

The analysis calculates signal based vetoes in the same manner that it does the coherent SNR: The necessary single detector filters are constructed and then these are combined together to create the χ^2 tests as described in the earlier sections.

Calculating the “standard” χ^2 test is computationally expensive. Therefore this veto is only calculated for a segment if there is at least one event within that segment with SNR larger than the threshold and with values of bank χ^2 , auto χ^2 and null SNR that do not immediately lead to it being dismissed as a glitch.

⁸ This choice stems from the desire to extend this search to incorporate a single spin. This is particularly appropriate for NSBH binaries where the spin of the NS can be safely neglected.

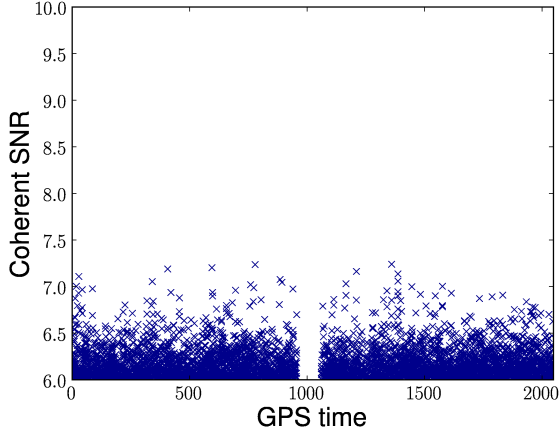


FIG. 7. The distribution of SNR triggers in the offsource region plotted against time for an analysis of simulated Gaussian noise in the initial LIGO (H1, H2, L1) network.

5. Simulated Signals

The sensitivity of the analysis to gravitational wave signals from CBC is assessed by adding simulated signals to the data stream before performing the search. The analysis uses the architecture from [60] to perform these simulations. A simulation is deemed to have been recovered by the analysis if there is an event within 0.1 seconds of the signal time; no attempt is made to guarantee a good match between simulated and recovered parameters. While this does mean that, in principle, signals may be found due to a nearby glitch, the effect is minimal, particularly when considering detection candidates which are louder than all background.

The results shown in the remainder of the section are based on a set of simulated signals comprised of binary neutron stars (component masses limited to be between 1 and $3 M_{\odot}$) at appropriate distances to be observable by the detector network. All of these binaries are oriented face on to the detectors. These choices are motivated by the fact that the current implementation is designed as a search for gravitational waves associated with GRBs.

B. Analysis of simulated data

The analysis was first run on simulated data for the initial LIGO network (H1, H2, L1). Data were simulated to be Gaussian and stationary, with no noise transients. Specifically, the coherent analysis pipeline was run on 2190 sections of Gaussian data as if a GRB had occurred in the middle of the data stretch. This provides a benchmark with which to compare results when running on real data.

Figure 7 shows all the triggers produced by the pipeline in the off source time. The loudest event in the approximately 2000 seconds of off-source data has an SNR of

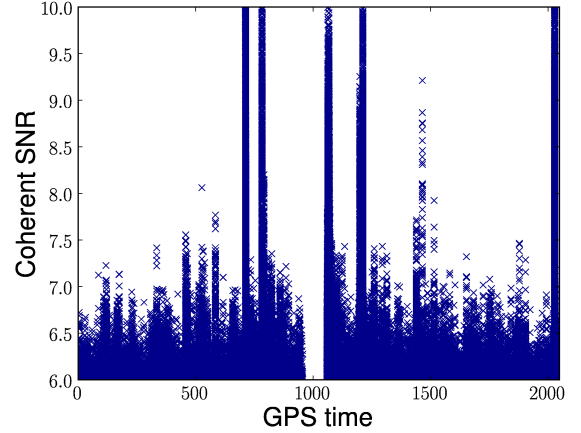


FIG. 8. The distribution of SNR triggers in the offsource region plotted against time for an analysis of a mock S4 GRB. The axes on the plot are chosen to be identical to those for figure 7 to make the plots easier to compare. The S4 data has a large number of non-Gaussian features. The largest of these peaks extends to a coherent SNR of 40, although non-Gaussian structure is visible at SNRs as low as 7.

7.24. Ideally, the various signal consistency tests described previously will reduce the amplitude of the loudest surviving event in real data to something similar to this.

C. Analysis of real data

A test analysis was performed on real data taken from S4. We chose an arbitrary block of 2190 seconds of data for which all three of the LIGO detectors were operating and ran the analysis as if a GRB had occurred during this time. The simulated sky location of the GRB was $(184.623^{\circ}, 42.294^{\circ})$ in right ascension and declination respectively. For this chosen time and sky location the sensitivity of the H1 and L1 detectors were roughly equal and the H2 detector was half as sensitive as the other two.

Coherent SNR

Figure 8 shows the coherent SNR of triggers produced during the analysis of the S4 data. It clearly demonstrates that this data is not well characterized by Gaussian noise alone. A number of loud transients are present in the data which show up as short duration peaks of large SNR. The loudest of these has an SNR of almost 40. If events were only ranked on SNR, a signal would have to be very loud to show against this non-Gaussian background. In addition to the loud peaks there are also a large number of quieter peaks that show up at all times in the data. If the search is to begin to approach the efficiency of the Gaussian case then the signal consistency

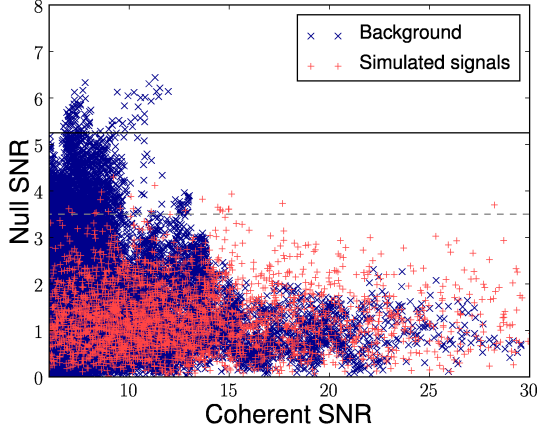


FIG. 9. The distribution of the null SNR plotted against coherent SNR. The solid line at null SNR of 5.5 is the line above which triggers are vetoed. The dashed line at 3.5 is the line above which triggers are downweighted (see section V C).

tests must allow us to reject the quieter noise transients, as well as the loud ones.

In the remainder of this subsection we demonstrate the performance of the signal consistency tests introduced in sections III and IV. Finally, we formulate a detection statistic, which arises as a combination of the coherent SNR and signal consistency tests, and demonstrate that with it the majority of the non-Gaussian background can be removed.

Null SNR

Figure 9 shows the performance of the null stream for both simulated signals and background noise. The ability of the null SNR to distinguish signal from noise is relatively poor in this example. The mock GRB analysis uses data from the two Hanford detectors and the detector at Livingston. Thus, the null stream is derived from a combination of the H1 and H2 detectors; the Livingston detector does not contribute. The loudest glitches during the time of this analysis originated in L1, and therefore do not have significant null SNR. However, quieter glitches in the Hanford detectors at an SNR around 10 do produce a large null SNR. Any trigger with a null SNR greater than 5 is eliminated from the analysis.

Single detector SNR

The most straightforward, and most effective amplitude consistency test we have found is the requirement of a single detector SNR greater than 4 in the two most sensitive detectors; In this analysis, the L1 and H1 detectors. Figure 10 demonstrates that this is a particularly effective strategy for removing noise glitches. Triggers

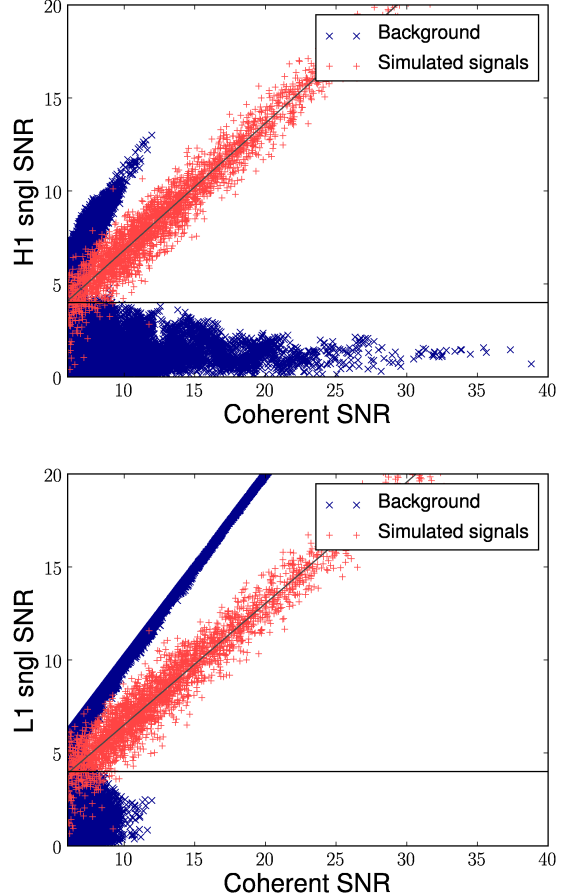


FIG. 10. The distribution of single detector SNR for the more sensitive H1 and L1 detectors, plotted against coherent SNR. The top figure shows the H1 SNR, the bottom figure shows the L1 SNR. The horizontal line indicates SNR=4. Below this line triggers will be vetoed. The inclined dark gray line indicates the expected SNR of these face on simulated signals.

arising due to glitches in the L1 detector have large coherent SNR but a negligible contribution from H1 and are consequently discarded.

χ^2 tests

In section IV we introduced three χ^2 tests designed to separate signals from noise glitches in the data. Figure 11 shows the distribution of the bank χ^2 for every time sample for a single template. This is directly comparable to Figure 3 which shows the same for Gaussian data. The deviation from the predicted χ^2 distribution is due to the non-Gaussianity of the data.

The distribution of bank and auto χ^2 for both simulated signals and noise triggers is shown in Figure 12. Both of these tests are effective at separating the simulated signals from noise transients. In order to quantify this, we make use of the *newSNR* formalism that

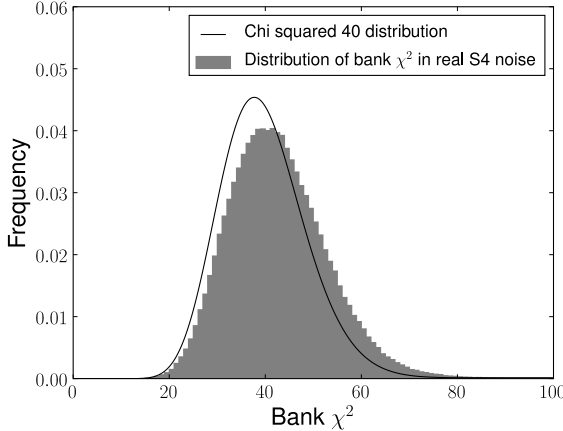


FIG. 11. The distribution of the bank χ^2 test for a single template h , with a bank of size 10. The plot shows the distribution of the bank veto calculated for every time sample in 128s of data. The observed distribution is inconsistent with the expected result in Gaussian noise (the black curve).

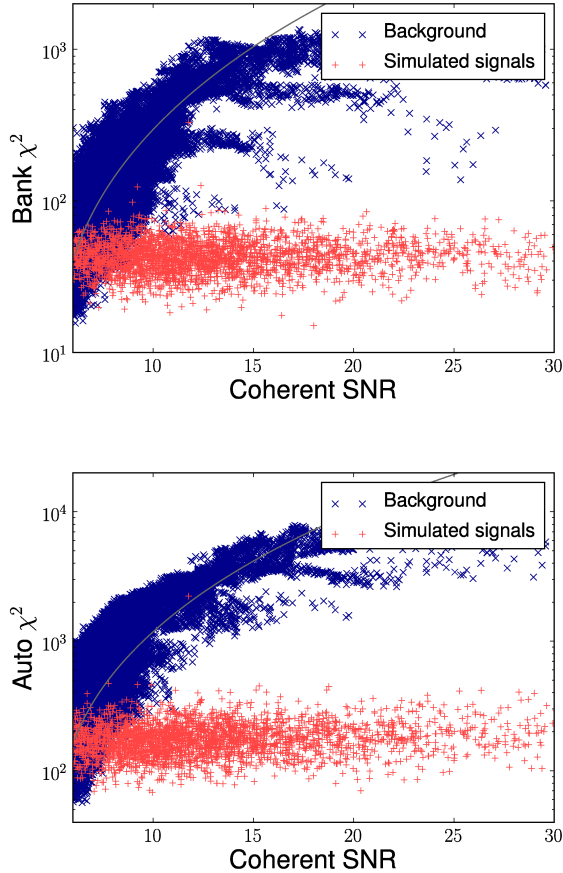


FIG. 12. The distribution of bank and auto χ^2 test plotted against SNR. The results for the off-source data triggers are plotted in blue, with simulated signals in red. The solid line shows the line of $newSNR = 6$, defined in section V C. Triggers with $newSNR < 6$ are vetoed.

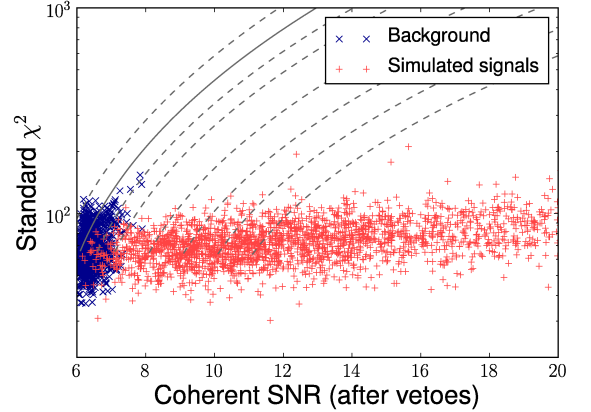


FIG. 13. The distribution of standard χ^2 test plotted against SNR. The results for the off-source data triggers are plotted in blue, with simulated signals in red. The dashed lines show contours of $newSNR$, defined in section V C, the solid line shows the line of $newSNR = 6$. Triggers with $newSNR < 6$ are vetoed.

is being used in the latest coincident searches for CBCs [64, 65]. The idea is to downweight the significance of noise triggers with large χ^2 values relative to signals. This is achieved by introducing the “ $newSNR$ ”:

$$\rho_{new} = \begin{cases} \rho, & \chi^2 \leq n_{dof} \\ \frac{\rho}{\left[\left(1 + \frac{\chi^2}{n_{dof}} \right)^{4/3} / 2 \right]^{1/4}}, & \chi^2 > n_{dof} \end{cases} \quad (5.1)$$

where n_{dof} is the number of degrees of freedom of the χ^2 test. For a signal, the mean χ^2 value is one per degree of freedom and consequently the $newSNR$ will be similar to the SNR. Noise transients with a large χ^2 value are significantly downweighted. The $newSNR$ is calculated using both the auto and bank χ^2 values. Any trigger with either an auto $newSNR$ or bank $newSNR$ less than 6 is discarded. The curves on Figure 12 show this $newSNR$ threshold for the two χ^2 tests.

Finally, we turn to the standard χ^2 test. As this is rather costly to compute, we only do so for triggers which have passed all of the previously described thresholds (on coherent, null and single detector SNR, the bank and auto χ^2). Figure 13 shows the distribution of the standard χ^2 test for simulated signals and noise. The preceding tests have succeeded in removing the vast majority of non-Gaussian triggers from the data. A threshold of 6 on $newSNR$ serves to eliminate a few more. We have found that the standard χ^2 is the most effective at separating signal from background so we also make use of it in the final ranking of events. Figure 13, shows contours of constant $newSNR$ which will be used in the final ranking.

Detection statistic

In the preceeding discussion, we have imposed a number of cuts on the initial candidate events produced by the analysis pipeline. Let us briefly recap those cuts:

- Generate a trigger at any time for which $\rho > 6$. Only keep the loudest one in each 0.1 seconds.
- Discard any triggers with $\rho_N > 5$.
- Discard any triggers for which $\rho_{H1} < 4$ or $\rho_{L1} < 4$.
- Discard any triggers for which $\rho_{new} < 6$ for the bank or auto χ^2 .

Finally, we rank the remaining triggers based upon the *newSNR* calculated using the standard χ^2 as well as the null SNR as:

- Rank remaining triggers using a detection statistic ρ_{det} given by

$$\rho_{det} = \begin{cases} \rho_{new}, & \rho_N \leq 3.5 \\ \frac{\rho_{new}}{\rho_{Null} - 2.5}, & 3.5 < \rho_N < 5.0 \end{cases} \quad (5.2)$$

The length of time a CBC spends in the sensitive band of the detector varies greatly with the mass, and it has been found that the shorter, high mass templates are more susceptible to occurring with large SNR at the time of glitches [66]. Also, the various signal consistency tests are less effective for these short templates. Therefore, we follow Ref. [66] and split the template bank into three regions based on the chirp mass of the template. The false alarm probability for a given trigger is based on a comparison of the detection statistic to off source triggers in the same mass bin.

Performance of search

The sensitivity of the analysis can be assessed by examining the performance of recovering simulated signals. The signal population was BNS with optimal orientation originating from the location of the fake GRB. For these purposes we will only consider an signal found if its associated trigger is louder than the loudest event that occurred in the low mass bin during the offsource time — this ensures that the false alarm probability is less than one in 324 (the number of offsource trials). At this level, a candidate event starts to be interesting but realistically a false alarm probability closer to 10^{-4} or 10^{-5} would be required for a detection candidate.

Figure 14 shows the efficiency with which simulated signals are recovered as a function of the distance. Recall that the largest SNR recorded in the analysis of simulated, Gaussian data was 7.24. We show the efficiency of the search at finding simulations with an SNR greater

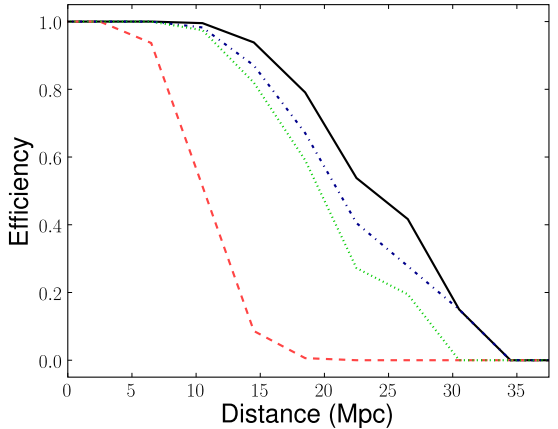


FIG. 14. Efficiency of recovery of simulated signals in real data. The efficiency is shown for four different cases: i) signals found above an SNR of 7.24, the loudest background trigger in Gaussian noise (black solid line); ii) signals found above an SNR of 12.88, the loudest background trigger in real noise (red dashed line); iii) signals found with a value of the detection statistic (5.2) above 7.41, the loudest background event; iv) signals found louder than all background in an H1-L1 search (green dotted line).

than this. If the data were Gaussian, or the signal consistency tests were able to remove all non-Gaussianities, then the real search would match this sensitivity. By using *only* SNR to rank events, the sensitivity of the search is substantially worse than in Gaussian data. Although the offsource contained events with an SNR up to 39, the loudest low mass trigger had a coherent SNR of 12.88. This is almost double the loudest Gaussian noise and thus the sensitivity of the search is reduced by about a factor of two — illustrated by the 50% efficiency moving down from 20 Mpc to 10 Mpc. The signal consistency tests — null stream, χ^2 tests and single detector SNR threshold — are designed to bring the sensitivity closer to the Gaussian case. The simulated signals are considered found if they are recovered with a detection SNR greater than 7.41 (the loudest off-source event) and all signal consistency tests. The efficiency of the detection search is only about 10% less than it would be in Gaussian noise. The 10% loss in sensitivity can be attributed to having a slightly louder offsource event (7.41 rather than 7.24) and a *small* loss of efficiency due to the various signal consistency checks.

To illustrate the benefits of a coherent search, we would like to compare the performance with a coincidence search. For the initial LIGO network, signals close to detection threshold would be unlikely to have passed any SNR threshold placed on the H2 detector. Specifically, for a signal with a coherent SNR of 7.5, the expected SNR in H2 would be around 2.5 which is a prohibitively low threshold. Therefore it is reasonable to compare the coherent search to a two detector, H1-L1 coincidence search. For a two detector search, the coher-

ent and coincident SNRs are equal, and the null stream test is not available. Consequently, the performance of two detector coherent and coincident searches should be comparable. Therefore, we present the results of an H1-L1 detector coherent search to give an indication of the performance of a coincidence search. The efficiency of this two detector search is also shown in Figure 14. The sensitivity of the two detector search is about a factor of 10% lower than the three detector coherent search. For a network of three approximately equally sensitive detectors, we would expect an even greater sensitivity improvement from employing coherent techniques.

VI. DISCUSSION

We have presented a formulation of a targeted coherent search for compact binary coalescences. For Gaussian noise, the coherent SNR would be ideal for separating signals from the noise background. However, since data from gravitational wave interferometers is neither Gaussian nor stationary, we have also discussed a number of methods of separating the non-stationary noise background from the signal population. These tests include various χ^2 tests, which were originally designed for use in single detectors. We have extended them to the network analysis and demonstrated their continued efficacy. Additionally, the coherent analysis allows for some additional tests which are not readily available in the coincidence case. The most significant of these is the null SNR which can be used to reject events which are not consistent with two gravitational wave polarizations. Additionally, we explored consistency tests between the recovered amplitudes of the gravitational wave and found that a simple SNR threshold on the two most sensitive detectors gave excellent results.

The analysis described in this paper has been implemented and in the final section we showed results of a test run. This made use of the S4 data from the LIGO detectors. Although the data was far from Gaussian, after the application of all of the signal consistency tests the results were remarkably close to what would be expected in Gaussian noise. This analysis is available to be used in searches for GW inspiral signals associated with GRBs in more recent LIGO and Virgo data, such as S6 and VSR2 and VSR3.

There are a number of ways in which this analysis could be enhanced to broaden its use and increase its sensitivity. First, a number of GRBs, particularly those observed by Fermi [67] and IPN [68] are not localized sufficiently accurately that the error box can be treated as a point on the sky. Thus, it would be nice to extend this analysis to allow for a region of the sky to be covered. This would require looping over the relevant sky points; incorporating the correct detector sensitivities $F_{+, \times}$ and time

delays. In principle, this would not greatly slow down the analysis as the majority of time is taken in performing the single detector filters and these would *not* need to be re-calculated. As well as looking at a patch on the sky, the analysis could be extended to cover the whole sky, as appropriate for an un-triggered search. This brings in a host of new complications which have been met and dealt with by other coherent search methods [44, 69]. In order to obtain a good estimate of the background for an all sky, un-triggered search we would need to implement background estimation and time shifting the data would likely be the best way to do this.

Since GRBs are thought to be rather tightly beamed, it is reasonable to take them as being face on, or close to. In this case, the gravitational waves are circularly polarized and there is, in effect, only a single polarization. This opens the possibility of limiting the signal space to just this one polarization and adding an extra “null” test. Alternatively, it should be possible to perform a Bayesian marginalization over the astrophysically expected distributions of the various parameters.

The progenitors of short GRBs are thought to be BNS or NSBH. The search we have described is ideal for the BNS case as the spins of the neutron stars are unlikely to have a significant effect on the waveform. However, when one of the components of the binary is a black hole, the spin could be large. Furthermore, the mass ratio is likely to be relatively large. In this case, the spin of the black hole can have a significant effect on the observed waveform [63]. Consequently, we would like to extend this search to incorporate spin effects. The infrastructure described in this paper can already accept spinning waveforms, but the implementation of signal based vetoes proves somewhat more complex. Work is underway on this [70].

ACKNOWLEDGEMENTS

The authors would like to thank Sukanta Bose, Duncan Brown, James Clark, Alex Dietz, Tom Dent, Nick Fotopoulos, Phil Hall, Ioannis Kamaretsos, Duncan Macleod, Laura Nuttall, Valeriu Predoi, Patrick Sutton, Bangalore Sathyaprakash, John Veitch and Alan Weinstein for useful discussion and helpful comments about this work. In this work IWH was supported by the Science and Technology Facilities Council, UK, studentship ST/F005954/1, SF was supported by the Royal Society. This paper has been given the internal LIGO Scientific Collaboration (LSC) document number P1000104.

[1] B. Abbott *et al.* (LIGO Scientific Collaboration), Reports on Progress in Physics, **72**, 076901 (2009), arXiv:0711.3041 [gr-qc].

[2] F. Acernese *et al.* (Virgo Scientific Collaboration), Class. Quant. Grav., **23**, S635 (2006).

[3] B. Willke (LIGO Scientific Collaboration), Class. Quant. Grav., **24**, S389 (2007).

[4] J. Abadie *et al.* (LIGO and Virgo Scientific Collaborations), Phys. Rev., **D82**, 102001 (2010), arXiv:1005.4655 [gr-qc].

[5] B. P. Abbott *et al.* (LIGO and Virgo Scientific Collaborations), Nature, **460**, 990 (2009), arXiv:0910.5772 [astro-ph.CO].

[6] J. Abadie *et al.* (LIGO and Virgo Scientific Collaborations), Phys. Rev., **D81**, 102001 (2010), arXiv:1002.1036 [gr-qc].

[7] B. Abbott *et al.* (LIGO and Virgo Scientific Collaborations), Astrophys. J., **713**, 671 (2010), arXiv:0909.3583 [astro-ph.HE].

[8] G. M. Harry (LIGO Scientific), Class. Quant. Grav., **27**, 084006 (2010).

[9] “Advanced LIGO,” <http://www.ligo.caltech.edu/advLIGO/>.

[10] “Advanced Virgo,” <http://www.cascina.virgo.infn.it/advirgo/>.

[11] J. Abadie *et al.* (LIGO and Virgo Scientific Collaborations), Class. Quant. Grav., **27**, 173001 (2010), arXiv:1003.2480 [astro-ph.HE].

[12] “LCGT: Large Scale Cryogenic Gravitational Wave Telescope,” <http://gw.icrr.u-tokyo.ac.jp/lcgt/>.

[13] “AIGO: Australian International Gravitational Observatory,” <http://www.aigo.org.au/>.

[14] S. Hild, S. Chelkowski, and A. Freise, (2008), arXiv:0810.0604 [gr-qc].

[15] B. Abbott *et al.* (LIGO Scientific Collaboration), Astrophys. J., **681**, 1419 (2008), arXiv:0711.1163 [astro-ph].

[16] J. Abadie *et al.* (LIGO and Virgo Scientific Collaborations), Astrophys. J., **715**, 1453 (2010), arXiv:1001.0165 [astro-ph.HE].

[17] B. P. Abbott *et al.* (LIGO and Virgo Scientific Collaborations), Astrophys. J., **715**, 1438 (2010), arXiv:0908.3824 [astro-ph.HE].

[18] J. Kanner *et al.*, Class. Quant. Grav., **25**, 184034 (2008), arXiv:0803.0312 [astro-ph].

[19] E. Nakar, Phys. Rept., **442**, 166 (2007), arXiv:astro-ph/0701748.

[20] M. Shibata and K. Taniguchi, Phys. Rev., **D77**, 084015 (2008), arXiv:0711.1410 [gr-qc].

[21] B. D. Metzger *et al.*, (2010), arXiv:1001.5029 [astro-ph.HE].

[22] V. Predoi *et al.*, Class. Quant. Grav., **27**, 084018 (2010), arXiv:0912.0476 [gr-qc].

[23] L. Blackburn *et al.*, Class. Quant. Grav., **25**, 184004 (2008), arXiv:0804.0800 [gr-qc].

[24] B. Allen, Phys. Rev., **D71**, 062001 (2005), arXiv:gr-qc/0405045.

[25] C. Hanna, *Searching for gravitational waves from binary systems in non-stationary data*, Ph.D. thesis, Louisiana State University (2008).

[26] Y. Guersel and M. Tinto, Phys. Rev., **D40**, 3884 (1989).

[27] B. P. Abbott *et al.* (LIGO Scientific Collaboration), Phys. Rev., **D80**, 047101 (2009), arXiv:0905.3710 [gr-qc].

[28] B. P. Abbott *et al.* (LIGO Scientific Collaboration), Phys. Rev., **D79**, 122001 (2009), arXiv:0901.0302 [gr-qc].

[29] A. Pai, S. Dhurandhar, and S. Bose, Phys. Rev., **D64**, 042004 (2001), arXiv:gr-qc/0009078.

[30] S. Bose, A. Pai, and S. V. Dhurandhar, Int. J. Mod. Phys., **D9**, 325 (2000), arXiv:gr-qc/0002010.

[31] S. Bose, S. V. Dhurandhar, and A. Pai, Pramana, **53**, 1125 (1999), arXiv:gr-qc/9906064.

[32] S. Bose, T. Dayanga, S. Ghosh, and D. Talukder, In preparation (2011).

[33] P. Jaranowski, A. Krolak, and B. F. Schutz, Phys. Rev., **D58**, 063001 (1998), arXiv:gr-qc/9804014.

[34] B. P. Abbott *et al.* (LIGO Scientific Collaboration), Phys. Rev., **D80**, 042003 (2009), arXiv:0905.1705 [gr-qc].

[35] C. Cutler and B. F. Schutz, Phys. Rev., **D72**, 063006 (2005), arXiv:gr-qc/0504011.

[36] N. J. Cornish and E. K. Porter, Class. Quant. Grav., **24**, 5729 (2007), arXiv:gr-qc/0612091.

[37] B. J. Owen and B. S. Sathyaprakash, Phys. Rev., **D60**, 022002 (1999), arXiv:gr-qc/9808076.

[38] J. C. Livas, *Upper limits for gravitational radiation from some astrophysical sources*, Ph.D. thesis, Massachusetts Institute of Technology (1987).

[39] L. A. Wainstein and V. D. Zubakov, *Extraction of Signals from Noise* (Prentice-Hall, Englewood Cliffs, 1962).

[40] R. Prix, Classical and Quantum Gravity, **24**, S481 (2007), arXiv:0707.0428 [gr-qc].

[41] T. Damour, B. R. Iyer, and B. S. Sathyaprakash, Phys. Rev., **D63**, 044023 (2001), arXiv:gr-qc/0010009.

[42] S. Klimenko, S. Mohanty, M. Rakhmanov, and G. Mitselmakher, Phys. Rev., **D72**, 122002 (2005), arXiv:gr-qc/0508068.

[43] S. Klimenko, S. Mohanty, M. Rakhmanov, and G. Mitselmakher, J. Phys. Conf. Ser., **32**, 12 (2006).

[44] P. J. Sutton *et al.*, New J. Phys., **12**, 053034 (2010), arXiv:0908.3665 [gr-qc].

[45] R. Prix and B. Krishnan, Class. Quant. Grav., **26**, 204013 (2009), arXiv:0907.2569 [gr-qc].

[46] C. A. K. Robinson, B. S. Sathyaprakash, and A. S. Sengupta, Phys. Rev., **D78**, 062002 (2008), arXiv:0804.4816 [gr-qc].

[47] B. Abbott *et al.* (LIGO Scientific Collaboration), Phys. Rev., **D72**, 082001 (2005), arXiv:gr-qc/0505041.

[48] L. Blanchet, Living Rev. Rel., **5**, 3 (2002), arXiv:gr-qc/0202016.

[49] M. Hannam *et al.*, Phys. Rev., **D79**, 084025 (2009), arXiv:0901.2437 [gr-qc].

[50] J. Abadie *et al.* (LIGO Scientific Collaboration), Nucl. Instrum. Meth., **A624**, 223 (2010), arXiv:1007.3973 [gr-qc].

[51] C. Van Den Broeck *et al.*, Phys. Rev., **D80**, 024009 (2009), arXiv:0904.1715 [gr-qc].

[52] D. Fazi, *Development of a physical-template search for gravitational waves from spinning compact-object binaries with LIGO*, Ph.D. thesis, Università di Bologna (2009).

[53] B. Abbott *et al.* (LIGO Scientific Collaboration), *Tuning matched filter searches for compact binary coalescence*, Tech. Rep. LIGO-T070109-01 (2007).

- [54] Y. Itoh, M. A. Papa, B. Krishnan, and X. Siemens, *Class. Quant. Grav.*, **21**, S1667 (2004), arXiv:gr-qc/0408092.
- [55] “LSC Algorithm Library Suite,” <https://www.lsc-group.phys.uwm.edu/daswg/projects/lalsuite.html>.
- [56] M. B. Davies, A. J. Levan, and A. R. King, *Mon. Not. Roy. Astron. Soc.*, **356**, 54 (2005), arXiv:astro-ph/0409681.
- [57] B. J. Owen, *Phys. Rev.*, **D53**, 6749 (1996), arXiv:gr-qc/9511032.
- [58] S. Babak, R. Balasubramanian, D. Churches, T. Cokelaer, and B. S. Sathyaprakash, *Class. Quant. Grav.*, **23**, 5477 (2006), arXiv:gr-qc/0604037.
- [59] T. Cokelaer, *Phys. Rev.*, **D76**, 102004 (2007), arXiv:0706.4437 [gr-qc].
- [60] B. P. Abbott *et al.* (LIGO Scientific Collaboration), *Phys. Rev.*, **D80**, 062001 (2009), arXiv:0905.1654 [gr-qc].
- [61] L. M. Goggin, (2008), arXiv:0908.2085 [gr-qc].
- [62] B. Allen, W. G. Anderson, P. R. Brady, D. A. Brown, and J. D. E. Creighton, (2005), arXiv:gr-qc/0509116.
- [63] Y. Pan, A. Buonanno, Y. Chen, and M. Vallisneri, *Phys. Rev.*, **D69**, 104017 (2004), erratum-*ibid.* **D74**, 029905(E) (2006), arXiv:gr-qc/0310034.
- [64] J. Abadie *et al.*, In preparation (2011).
- [65] J. Abadie *et al.*, In preparation (2011).
- [66] B. Abbott *et al.* (LIGO Scientific Collaboration), *Phys. Rev.*, **D79**, 122001 (2009).
- [67] “Fermi Gamma-ray space telescope,” http://www.nasa.gov/mission_pages/GLAST/science/index.html.
- [68] “The Interplanetary Network Progress Report,” <http://ipnpr.jpl.nasa.gov/index.cfm>.
- [69] S. Klimenko, I. Yakushin, A. Mercer, and G. Mitselmakher, *Class. Quant. Grav.*, **25**, 114029 (2008), arXiv:0802.3232 [gr-qc].
- [70] I. Harry and S. Fairhurst, (2010), in Preparation.